

Nonconvex Regularized Gradient Projection Sparse Reconstruction for Massive MIMO Channel Estimation

Pengxia Wu and Julian Cheng, *Senior Member, IEEE*

Abstract

Novel sparse reconstruction algorithms are proposed for beamspace channel estimations in massive multiple-input multiple-output systems. The proposed algorithms minimize a least-squares objective with a nonconvex regularizer. This regularizer removes the penalties on a few large-magnitude elements from the conventional ℓ_1 -norm regularizer, and thus it only forces penalties on the remaining elements that are expected to be zeros. Accurate and fast reconstructions can be achieved by performing gradient projection updates in a difference of convex functions (DC) programming framework. A double-loop algorithm and a single-loop algorithm are derived by different DC decompositions, and they have distinct computation complexities and convergence rates. An extension algorithm is further proposed to generalize the step size of the single-loop algorithm. This extension algorithm has a faster convergence rate and can achieve the same level of accuracy as the proposed double-loop algorithm. Numerical results show significant advantages of the proposed algorithms over the existing reconstruction algorithms in terms of reconstruction accuracies and runtimes.

Index Terms

DC programming, gradient projection, massive MIMO, nonconvex optimization, sparse channel reconstruction

I. INTRODUCTION

As a key technology for the fifth-generation and beyond communication systems, massive multiple-input multiple-output (MIMO) highly relies on accurate knowledge of channel state

P. Wu and J. Cheng are with the School of Engineering, The University of British Columbia, Kelowna, BC V1X 1V7, Canada (e-mail: pengxia.wu@alumni.ubc.ca, julian.cheng@ubc.ca).

information (CSI) to reap potential performance benefits from a large number of antennas. However, acquiring downlink CSI in a resource-efficient manner is problematic for frequency division duplex (FDD) systems, which occupy different spectrum bands in uplink and downlink channels. For such a system, downlink channels are estimated at the user equipments (UEs) and then the UEs send back the estimated CSI to the base station (BS); both the overheads of downlink pilots and CSI feedback are proportional to the number of BS antennas, which is large for massive MIMO. To reduce the overhead of downlink CSI acquisition, one can develop sparse channel estimation methods by exploiting channel sparsity in certain domains, since the unknown massive MIMO channels can be represented as high-dimensional sparse vectors in certain basis [1]. Based on a valid sparse representation of massive MIMO channel, transmitting pilots through massive MIMO channel can be regarded as a linear mapping of sparse channel vectors onto a compact subspace to obtain lower-dimensional observations. The full-dimensional channel vectors are then reconstructed at the BS. In such sparse channel estimation methods, the length of pilot sequence for each antenna is no longer proportional to the number of BS antennas, but only depends on the sparsity level of the channel. Therefore, the pilot sequence length is allowed to be much less than the number of BS antennas, and the downlink CSI acquisition overhead for FDD massive MIMO can be substantially reduced.

Sparse channel estimation [2] has been proposed for many traditional communication applications such as orthogonal frequency-division multiplexing systems [3], ultra-wideband communications [4], pulse-shaping multicarrier systems [5] and underwater acoustic communications [6]. Channels in these applications have sparse impulse responses because a multipath channel has a large delay spread and only a small number of nonzero taps [2]. Nowadays, sparse channel estimation has been increasingly investigated for massive MIMO systems, and various beamspace channel estimation schemes have been developed for massive MIMO systems [7]–[16]. Due to a limited number of scattering clusters and small angular spread for each scattering cluster, the massive MIMO angular-domain (beamspace) channel exhibits a sparse characteristic [17], i.e., a majority of channel energy is occupied by a few dimensions and most elements in beamspace channel vectors are either zero or nearly zero. More recently, owing to the strong sparsity of millimeter-wave (mmWave) channels, sparse channel estimation becomes popular in mmWave massive MIMO systems with a hybrid analog-and-digital (AD) architecture [18], where full-dimensional channel vectors have to be estimated from a few number of observations due to a limited number of radio-frequency chains [18]–[21].

Sparse channel estimation requires to reconstruct high-dimensional sparse channel vectors from lower-dimensional observations. An efficient sparse reconstruction algorithm is essential to achieve accurate channel estimations. The ultimate sparse reconstruction problem is an ℓ_0 -minimization optimization problem, which is NP hard [22]. Alternatively, one can replace the ℓ_0 -norm by other simple functions to seek approximate solutions. The most popular method is to use the ℓ_1 -norm to approximate the ℓ_0 -norm, and this method is known as ℓ_1 -relaxation or convex relaxation. Several well-known ℓ_1 -relaxation algorithms have been proposed such as the $l1_ls$ [23], Bregman iterative regularization [24], gradient projection for sparse reconstruction (GPSR) [25], sparse reconstruction by separable approximation (SpaRSA) [26], iterative shrinkage-thresholding algorithm (ISTA) [27] and the fast iterative shrinkage-thresholding algorithm (FISTA) [28]. These ℓ_1 -relaxation algorithms have theoretical convergence guarantees, but an ℓ_1 -norm is a loose approximation of ℓ_0 -norm and it can lead to biased estimates. To achieve tighter approximations, several nonconvex functions have been proposed, including the ℓ_q -norm for $0 \leq q \leq 1$ [29] and the difference of two continuous functions [30]. Another popular method is the greedy approach, and representative algorithms include orthogonal matching pursuit (OMP) [31], [32], CoSaMP [33] and the least angle regression (LARS) [34]. Greedy methods work well for sufficiently sparse vectors, but their reconstruction accuracies and speeds degrade severely when sparsity reduces.

In this paper, we propose to use the difference of convex functions (DC) programming and gradient projection descent algorithm to solve sparse channel reconstructions in massive MIMO systems. Instead of approximating the ℓ_0 -norm, we exactly represent the ℓ_0 -norm constraint by introducing the top- $(K, 1)$ norm [35]¹, which is simply the sum of K largest elements of a vector in terms of absolute values. Thus, the original ℓ_0 -minimization sparse reconstruction problem can be equivalently transformed into a least squares optimization penalised by a nonconvex regularizer. The regularizer is more favorable than the ℓ_1 -regularizer because it removes the penalties on large-magnitude elements, but it leads to a nonconvex optimization problem. We adopt the DC programming framework to transform the nonconvex problem into a list of convex subproblems, and apply gradient projection descent method to solve these convex subproblems. We propose three different DC gradient projection sparse reconstruction (DC-GPSR) algorithms.

¹Although the top- $(K, 1)$ norm and a DC programming algorithm employing the soft thresholding operation were proposed to solve several ℓ_0 -constrained optimization problems [35], the sparse reconstruction problem has not been investigated therein.

The proposed algorithms are distinct in terms of time complexities, but they can achieve the same level of reconstruction accuracy. The contributions of this paper are summarized as follows:

- We propose a double-loop DC-GPSR algorithm (Algorithm 1), which applies gradient projection descent in a DC programming framework. Our preliminary study has reported this highly accurate, simple and robust algorithm [36]. However, the double-loop mechanism of Algorithm 1 can be criticized for less efficiency; therefore, in this paper, we further propose the single-loop algorithms.
- We apply a special DC decomposition on the objective function such that the convex subproblem in the DC programming has a closed-form solution. Thus, we propose a single-loop DC-GPSR algorithm (Algorithm 2), which can avoid inner loops and solve the DC programming subproblem in a one-step update.
- We find that an update of the single-loop DC-GPSR algorithm can be interpreted as a gradient projection descent update with a required step size. Thus, we adopt the Barzilai-Borwein (BB) step size to generalize the basic single-loop DC-GPSR algorithm and propose Algorithm 3 that improves convergence significantly.

II. SYSTEM MODEL

We consider a downlink massive MIMO system having N_t transmit antennas at the BS and N_r receiver antennas at the UE. Assuming a slowly time-varying narrowband multipath channel, the physical channel can be represented by [37]

$$\mathbf{H}_s = \sqrt{N_r N_t} \sum_{l=1}^{N_p} \alpha_l \boldsymbol{\alpha}_r(\theta_{r,l}) \boldsymbol{\alpha}_t^H(\theta_{t,l}) \quad (1)$$

where $\mathbf{H}_s \in \mathbb{C}^{N_r \times N_t}$ is the channel matrix, p denotes the multipath index, N_p is the number of paths, α_p is the complex channel gain of the p th path, $\boldsymbol{\alpha}_r(\theta_{r,p})$ and $\boldsymbol{\alpha}_t(\theta_{t,p})$ are respectively the array steering vectors² of receiver and transmitter array for the p th path, and the corresponding angle of arrival (AoA) and the angle of departure (AoD) are $\theta_{r,p}$ and $\theta_{t,p}$. For a one-dimensional uniform linear array (ULA) consisting of N elements, the steering vector can be expressed as $\boldsymbol{\alpha}(\theta) = [1, e^{-j2\pi\vartheta}, e^{-j4\pi\vartheta}, \dots, e^{-j2\pi\vartheta(N-1)}]^T$, where $\vartheta \in [-1, 1]$ is the normalized spatial angle, which is related to the physical angle $\theta \in [-\pi/2, \pi/2]$ by $\vartheta = \frac{d}{\lambda} \sin(\theta)$, and where $d = \lambda/2$ is the antenna spacing and λ is the wavelength.

²Array steering vector represents the array phase profile as a function of physical AoA or AoD.

The spatial domain channel matrix \mathbf{H}_s can be transformed into the beamspace channel matrix \mathbf{H}_a via a two-dimensional Fourier transform [17]

$$\mathbf{H}_a = \mathbf{U}_r^H \mathbf{H}_s \mathbf{U}_t \quad (2)$$

where $\mathbf{U}_t \in \mathbb{R}^{N_t \times N_t}$ and $\mathbf{U}_r \in \mathbb{R}^{N_r \times N_r}$ are unitary digital Fourier transform (DFT) matrices, which can be expressed using array steering vectors as $\mathbf{U}_t = \frac{1}{\sqrt{N_t}} [\boldsymbol{\alpha}_t(\theta_{t,0}), \boldsymbol{\alpha}_t(\theta_{t,1}), \dots, \boldsymbol{\alpha}_t(\theta_{t,N_t-1})]^T$, $\mathbf{U}_r = \frac{1}{\sqrt{N_r}} [\boldsymbol{\alpha}_r(\theta_{r,0}), \boldsymbol{\alpha}_r(\theta_{r,1}), \dots, \boldsymbol{\alpha}_r(\theta_{r,N_r-1})]^T$, where $\{\theta_{t,0}, \dots, \theta_{t,N_t-1}\}$ and $\{\theta_{r,0}, \dots, \theta_{r,N_r-1}\}$ are the virtual AoDs and AoAs defined by array elements of transmitter and receiver. Beamspace channel \mathbf{H}_a is sparse due to the limited number of scattering clusters and high dimensionality of massive MIMO channels [37]. In practice, owing to the limited resolution of the virtual angular grids $(\theta_{r,i}, \theta_{t,j})$ for $0 \leq i \leq N_r-1$ and $0 \leq j \leq N_t-1$, mismatches often happen between the predefined virtual angular grid and the real-path AoA and AoD $(\theta_{r,l}, \theta_{t,l})$ for $l \in \{1, \dots, N_p\}$. This phenomenon is known as power leakage, which can cause beamspace channels being not exactly sparse. However, for a massive MIMO system having hundreds of antennas, power leakage can be neglected since the energy (square sum) of a few largest-magnitude elements can capture most of the channel power $\|\mathbf{H}_a\|_2^2$ [38]. In this case, the beamspace channel is approximately sparse or compressible.

By transmitting the known pilots \mathbf{P} from the BS through channel, the UE receives pilot observations as

$$\mathbf{R} = \mathbf{H}_s \mathbf{P} + \mathbf{W} \quad (3)$$

where $\mathbf{R} \in \mathbb{C}^{N_r \times L}$ is the received pilot observations, and where L is the length of pilots for each antenna; $\mathbf{H}_s \in \mathbb{C}^{N_r \times N_t}$ is the spatial-domain channel matrix, $\mathbf{P} \in \mathbb{C}^{N_t \times L}$ is the transmitted pilot matrix; $\mathbf{W} \in \mathbb{C}^{N_r \times L}$ is the additive white Gaussian noise (AWGN) matrix whose elements are independent identical distributed (i.i.d.) complex Gaussian random variables having mean zero and variance σ_n^2 . Conventional linear reconstruction methods such as linear minimum mean square error (LMMSE) or least square (LS) requires $L \geq N_t$ to estimate the channel accurately. When the number of antenna elements N_t is large, the pilot-length requirement implies unbearable spectral occupancy and computation complexity. On the contrary, beamspace channel estimation is attractive because the sparse beamspace channel $\hat{\mathbf{H}}_s$ can be accurately reconstructed even when $L \ll N_t$.

From the transformation between spatial domain channel \mathbf{H}_s and beamspace channel \mathbf{H}_a in (2), we have $\mathbf{H}_s = \mathbf{U}_r \mathbf{H}_a \mathbf{U}_t^H$. Thus, eq. (3) can be expressed as

$$\mathbf{R} = \mathbf{U}_r \mathbf{H}_a \mathbf{U}_t^H \mathbf{P} + \mathbf{W}. \quad (4)$$

By taking conjugate transposes and right multiplications with \mathbf{U}_r on both sides of (4), we have

$$\mathbf{R}^H \mathbf{U}_r = \mathbf{P}^H \mathbf{U}_t \mathbf{H}_a^H \mathbf{U}_r^H \mathbf{U}_r + \mathbf{W}^H \mathbf{U}_r \quad (5)$$

By representing $\mathbf{R}' = \mathbf{R}^H \mathbf{U}_r$, $\mathbf{A} = \mathbf{P}^H \mathbf{U}_t$, $\mathbf{H} = \mathbf{H}_a^H$ and $\mathbf{W}' = \mathbf{W}^H \mathbf{U}_r$, we can simplify (5) as

$$\mathbf{R}' = \mathbf{A} \mathbf{H} + \mathbf{W}' \quad (6)$$

where $\mathbf{R}' \in \mathbb{C}^{L \times N_r}$, $\mathbf{A} \in \mathbb{C}^{L \times N_t}$, $\mathbf{H} \in \mathbb{C}^{N_t \times N_r}$ and $\mathbf{W}' \in \mathbb{C}^{L \times N_r}$. For the i th ($1 \leq i \leq N_r$) column of \mathbf{R}' , \mathbf{H} and \mathbf{W}' in (6), we have

$$\mathbf{r}'_i = \mathbf{A} \mathbf{h}_i + \mathbf{w}'_i. \quad (7)$$

We adopt the real-form matrix \mathbf{A} by forcing the imaginary part of \mathbf{A} to be zeros, i.e., $\Im(\mathbf{A}) = \mathbf{0}$, $\mathbf{A} = \Re(\mathbf{A})$, where $\Re(\cdot)$ and $\Im(\cdot)$ respectively denote the real and imaginary part of a complex vector. Thus, the computation complexity can be reduced to a half of the original complex-valued matrix-vector multiplication of $\mathbf{A} \mathbf{h}_i$. We stack the real part the imaginary part of the complex channel vector \mathbf{h}_i , and express (7) as

$$\begin{bmatrix} \Re(\mathbf{r}'_i) \\ \Im(\mathbf{r}'_i) \end{bmatrix} = \begin{bmatrix} \Re(\mathbf{A}) & \mathbf{0} \\ \mathbf{0} & \Re(\mathbf{A}) \end{bmatrix} \begin{bmatrix} \Re(\mathbf{h}_i) \\ \Im(\mathbf{h}_i) \end{bmatrix} + \begin{bmatrix} \Re(\mathbf{w}'_i) \\ \Im(\mathbf{w}'_i) \end{bmatrix}. \quad (8)$$

We write the stacked channel vector as $\mathbf{x} = [\Re(\mathbf{h}_i)^T, \Im(\mathbf{h}_i)^T]^T$, and express (8) as

$$\mathbf{y} = \Phi \mathbf{x} + \mathbf{n} \quad (9)$$

where $\mathbf{y} = [\Re(\mathbf{r}'_i)^T, \Im(\mathbf{r}'_i)^T]^T$, $\Phi = \begin{bmatrix} \Re(\mathbf{A}) & \mathbf{0} \\ \mathbf{0} & \Re(\mathbf{A}) \end{bmatrix}$, and $\mathbf{n} = [\Re(\mathbf{w}'_i)^T, \Im(\mathbf{w}'_i)^T]^T$. In the remainder of this paper, we uniquely refer the real-form vector \mathbf{x} as the sparse channel vector. The goal of beamspace channel estimation is to reconstruct sparse channel vector $\hat{\mathbf{x}}$ given a known measurement matrix Φ and measurements \mathbf{y} such that $\hat{\mathbf{x}} \approx \mathbf{x}$ by solving the underdetermined linear system (9).

III. DC REPRESENTATION FOR SPARSE CONSTRAINT

In this section, We first briefly review the conventional ℓ_1 -norm regularized least squares for solving sparse reconstructions. Then, we introduce the top- $(K, 1)$ norm [35] to represent the ℓ_0 -norm constraint exactly in a sparse reconstruction problem. Also, we provide a threshold to determine the penalty parameter.

According to (9), reconstructing \mathbf{x} from \mathbf{y} and Φ using the sparsity as a prior is an NP-hard ℓ_0 -minimization problem, which is defined as [39]

$$\begin{aligned} \min_{\mathbf{x}} \quad & \|\mathbf{x}\|_0 \\ \text{s.t.} \quad & \|\mathbf{y} - \Phi\mathbf{x}\|_2^2 \leq \tau \end{aligned} \quad (10)$$

where τ is a nonnegative real-form parameter. The problem (10) can be rewritten in an equivalent form as [39]

$$\begin{aligned} \min_{\mathbf{x}} \quad & \|\mathbf{y} - \Phi\mathbf{x}\|_2^2 \\ \text{s.t.} \quad & \|\mathbf{x}\|_0 \leq K \end{aligned} \quad (11)$$

where K is the bound of the number of nonzero elements of vector \mathbf{x} , and it is uniquely determined by the parameter τ in problem (10).

A more common method to solve problem (11) is by the ℓ_1 -relaxation that replaces the nonconvex ℓ_0 -norm $\|\mathbf{x}\|_0$ by the convex ℓ_1 -norm $\|\mathbf{x}\|_1$ as

$$\begin{aligned} \min_{\mathbf{x}} \quad & \|\mathbf{y} - \Phi\mathbf{x}\|_2^2 \\ \text{s.t.} \quad & \|\mathbf{x}\|_1 \leq t \end{aligned} \quad (12)$$

where t is a nonnegative real parameter that controls the sparsity level of the reconstruction vector. Using an appropriate multiplier $\lambda \geq 0$, problem (12) can be rewritten in an equivalent form as

$$\min_{\mathbf{x}} \frac{1}{2} \|\mathbf{y} - \Phi\mathbf{x}\|_2^2 + \lambda \|\mathbf{x}\|_1 \quad (13)$$

where $\lambda \geq 0$ is a penalty parameter to balance the data-fidelity and regularization. The penalty parameter λ is difficult to tune, since the ℓ_1 -regularizer $\lambda\|\mathbf{x}\|_1$ forces equal penalties on each element of \mathbf{x} . A larger λ will force a sparser solution $\hat{\mathbf{x}}$ but can increase the residual error $\|\mathbf{y} - \Phi\hat{\mathbf{x}}\|_2^2$, whereas a small λ will lead to a solution that is insufficiently sparse. Cross-validation is a common approach to find a proper value of λ , but it is computationally intensive for

large-scale problems. Sometimes, it is impractical to select a proper parameter by cross-validation owing to a large number of distinct instances.

In contrast to using ℓ_1 -relaxation, we introduce the top- $(K, 1)$ norm so that the constraint $\|\mathbf{x}\|_0 \leq K$ in the original problem (11) can be expressed exactly. The top- $(K, 1)$ norm $\|\mathbf{x}\|_{K,1}$ is defined as the sum of the largest K elements of the vector \mathbf{x} in terms of absolute value, namely

$$\|\mathbf{x}\|_{K,1} := |x_{(1)}| + |x_{(2)}| + \cdots + |x_{(K)}| \quad (14)$$

where $|x_{(i)}|$ denotes the element whose absolute value is the i th-largest among the N elements of the vector \mathbf{x} , i.e., $|x_{(1)}| \geq |x_{(2)}| \geq \cdots \geq |x_{(N)}|$. The constraint $\|\mathbf{x}\|_0 \leq K$ is equivalent to the statement that the $(K+1)$ th-largest element of the vector \mathbf{x} is zero, i.e., $\|\mathbf{x}\|_{K+1,1} - \|\mathbf{x}\|_{K,1} = 0$. Thus, we have an equivalent relationship between the following two statements [35]

$$\|\mathbf{x}\|_0 \leq K \Leftrightarrow \|\mathbf{x}\|_1 - \|\mathbf{x}\|_{K,1} = 0. \quad (15)$$

Since both $\|\mathbf{x}\|_1$ and $\|\mathbf{x}\|_{K,1}$ are convex, we say the equality $\|\mathbf{x}\|_1 - \|\mathbf{x}\|_{K,1} = 0$ is an exact DC representation for sparsity constraint. By replacing the sparsity constraint $\|\mathbf{x}\|_0 \leq K$ in (11) using exact DC constraint $\|\mathbf{x}\|_1 - \|\mathbf{x}\|_{K,1} = 0$, the sparse reconstruction problem can be rewritten as

$$\begin{aligned} \min_{\mathbf{x}} \quad & \|\mathbf{y} - \Phi\mathbf{x}\|_2^2 \\ \text{s.t.} \quad & \|\mathbf{x}\|_1 - \|\mathbf{x}\|_{K,1} = 0. \end{aligned} \quad (16)$$

Using an appropriate Lagrange multiplier ρ , we obtain the following unconstrained optimization problem from the problem (16)

$$\min_{\mathbf{x}} \quad \frac{1}{2} \|\mathbf{y} - \Phi\mathbf{x}\|_2^2 + \rho(\|\mathbf{x}\|_1 - \|\mathbf{x}\|_{K,1}) := F(\mathbf{x}) \quad (17)$$

where ρ is the regularization parameter that balances the data consistency and penalty term. Our formulated optimization problem (17) differs from the conventional ℓ_1 -regularized sparse reconstruction (13) only in terms of the subtracted top- $(K, 1)$ norm $\|\mathbf{x}\|_{K,1}$ in penalty term³. The regularizer $\rho(\|\mathbf{x}\|_1 - \|\mathbf{x}\|_{K,1})$ is better than an ℓ_1 -norm regularizer because it removes the penalties on the K largest-magnitude elements.

³In practice, if the sparsity level of reconstructing vector is already known, we set K as the number of nonzero elements of reconstruction vectors; if the sparsity level of reconstructing vector is unknown, we can use cross validation to determine K .

To ensure the equivalence between the unconstrained problem (17) and the constraint problem (16), we provide a threshold ρ^* for the penalty parameter selection in Theorem 1.

Theorem 1: Let \mathbf{x}_{ρ^*} be an optimal solution of (17) with given ρ^* . Suppose there exists a constant $q > 0$ such that $\|\mathbf{x}_{\rho^*}\|_2 \leq q$ for any $\rho^* > 0$. Then \mathbf{x}_{ρ^*} is also optimal to (16) if

$$\rho^* \geq \max_i \{q(\|\Phi^T \Phi \mathbf{e}_i\|_2 + |(\Phi^T \Phi)_{ii}|/2) + |(\Phi^T \mathbf{y})_i|\}$$

where $1 \leq i \leq N_t$; \mathbf{e}_i represents the unit vector in which the i th element is one while the other elements are zeros; $(\Phi^T \Phi)_{ii}$ represents the i th diagonal elements of matrix $\Phi^T \Phi$; $(\Phi^T \mathbf{y})_i$ indicates the i th element of the vector $\Phi^T \mathbf{y}$.

Prove: See Appendix A.

IV. DOUBLE-LOOP DC GRADIENT PROJECTION DESCENT FOR SPARSE RECONSTRUCTION

We have formulated the sparse reconstructions into a nonconvex optimization problem (17). In this section, we use DC programming and gradient projection descent to solve problem (17). We will propose a double-loop DC-GPSR algorithm.

A. DC Programming Framework

The DC programming is an iterative algorithm framework that can ensure global convergence [22]. For a nonconvex unconstrained optimization problem

$$\min_{\mathbf{x}} f(\mathbf{x}) - g(\mathbf{x}) \quad (18)$$

where $f(\mathbf{x})$ and $g(\mathbf{x})$ are two convex functions. The DC programming method solves the following convex subproblem at the t th-iteration,

$$\min_{\mathbf{x}} f(\mathbf{x}) - \mathbf{x}^T \partial g(\mathbf{x}^{t-1}) \quad (19)$$

where the second convex function $g(\mathbf{x})$ in (18) is linearized by $\mathbf{x}^T \partial g(\mathbf{x}^{t-1})$ in (19), and where $\partial g(\mathbf{x}^{t-1})$ represents the gradient (or subgradient) of $g(\mathbf{x}^{t-1})$ with respect to \mathbf{x}^{t-1} . The DC algorithm framework can be outlined as follows:

1. **Start:** Given a starting point \mathbf{x}^0 , and a small threshold parameter $\epsilon > 0$.
2. **Repeat:** For $t = 1, 2, \dots$
 - Compute the gradient (or subgradient) $\partial g(\mathbf{x}^{t-1})$
 - Solve the convex subproblem (19) for obtaining \mathbf{x}^t
3. **End:** Until a terminate condition is satisfied.

B. A Double-Loop DC-GPSR Algorithm

Following the DC programming framework, we decompose our objective function in (17) as the difference of the two convex functions of $f(\mathbf{x})$ and $g(\mathbf{x})$

$$\min_{\mathbf{x}} \underbrace{\frac{1}{2} \|\mathbf{y} - \Phi \mathbf{x}\|_2^2 + \rho \|\mathbf{x}\|_1}_{f(\mathbf{x})} - \underbrace{\rho \|\mathbf{x}\|_{K,1}}_{g(\mathbf{x})}. \quad (20)$$

At the t th-iteration, we solve the following convex subproblem

$$\min_{\mathbf{x}} f(\mathbf{x}) - \rho \mathbf{x}^T \partial \|\mathbf{x}^{t-1}\|_{K,1} \quad (21)$$

where $\partial \|\mathbf{x}^{t-1}\|_{K,1}$ denotes the subgradient of top- $(K, 1)$ norm for \mathbf{x}^{t-1} , and where the superscript $t-1$ indicates the $(t-1)$ th update. The subgradient of top- $(K, 1)$ norm $\partial \|\mathbf{x}\|_{K,1}$ for \mathbf{x} is defined as [35]

$$\partial \|\mathbf{x}\|_{K,1} := \operatorname{argmax}_{\mathbf{w}} \left\{ \sum_{i=1}^N x_i w_i \mid \sum_{i=1}^N |w_i| = K, w_i \in [-1, 1] \right\}. \quad (22)$$

By substituting the $f(\mathbf{x})$ and using \mathbf{w}_x^{t-1} to denote a feasible value for the subgradient $\partial \|\mathbf{x}^{t-1}\|_{K,1}$, we write the subproblem (21) as

$$\min_{\mathbf{x}} \frac{1}{2} \|\mathbf{y} - \Phi \mathbf{x}\|_2^2 + \rho \|\mathbf{x}\|_1 - \rho \mathbf{x}^T \mathbf{w}_x^{t-1} \quad (23)$$

where $\mathbf{w}_x^{t-1} \in \partial \|\mathbf{x}^{t-1}\|_{K,1}$. A feasible subgradient \mathbf{w}_x^{t-1} can be simply obtained by setting the signs of the first K largest elements of $|\mathbf{x}^{t-1}|$ to the corresponding elements of \mathbf{w}_x^{t-1} , i.e., $(\mathbf{w}_x^{t-1})_{(i)} = \operatorname{sign}(x_{(i)}^{t-1})$, and setting the other elements of \mathbf{w}_x^{t-1} to be zeros, where the subscript i indicates the i th element of a vector.

We obtain a convex subproblem (23). We will turn (23) into a constraint quadratic problem so that we can solve it using the gradient projection descent method. Specifically, we split the positive and negative part of \mathbf{x} , and represent \mathbf{x} as the difference of its positive part \mathbf{u} and its negative part \mathbf{v} , that is

$$\mathbf{x} = \mathbf{u} - \mathbf{v}, \quad \mathbf{u} \geq \mathbf{0}, \mathbf{v} \geq \mathbf{0}. \quad (24)$$

where $\mathbf{u} = (\mathbf{x})_+$, $\mathbf{v} = (-\mathbf{x})_+$, where $(\cdot)_+$ is the positive-taking operation that retains the positive elements and sets the other elements be zeros. More precisely, $(\mathbf{x})_+$ represents for each element x in vector \mathbf{x} we take $(x)_+ = \max\{0, x\}$; $(-\mathbf{x})_+$ represents for each element $-x$ in vector $-\mathbf{x}$

we take $(-x)_+ = \max\{0, -x\}$. Noticing that $\|\mathbf{x}\|_1 = \mathbf{1}^T \mathbf{u} + \mathbf{1}^T \mathbf{v}$, the subproblem (23) can be written as a bound-constrained quadratic program (BCQP)

$$\begin{aligned} \min_{\mathbf{u}, \mathbf{v}} \quad & \frac{1}{2} \|\mathbf{y} - \Phi(\mathbf{u} - \mathbf{v})\|_2^2 + \rho \mathbf{1}^T \mathbf{u} + \rho \mathbf{1}^T \mathbf{v} - \rho \mathbf{u}^T \mathbf{w}_u^{t-1} - \rho \mathbf{v}^T \mathbf{w}_v^{t-1} \\ \text{s.t.} \quad & \mathbf{u} \geq \mathbf{0}, \mathbf{v} \geq \mathbf{0} \end{aligned} \quad (25)$$

where \mathbf{w}_u^{t-1} and \mathbf{w}_v^{t-1} respectively represent the positive and negative part of \mathbf{w}_x^{t-1} , i.e., $\mathbf{w}_u^{t-1} = (\mathbf{w}_x^{t-1})_+$, $\mathbf{w}_v^{t-1} = (-\mathbf{w}_x^{t-1})_+$. Let \mathbf{z} denote the concatenation of \mathbf{u} and \mathbf{v} , i.e., $\mathbf{z} = [\mathbf{u}^T, \mathbf{v}^T]^T$, we rewrite (25) into a compact form

$$\begin{aligned} \min_{\mathbf{z}} \quad & \frac{1}{2} \mathbf{z}^T \mathbf{B} \mathbf{z} + \mathbf{c}^T \mathbf{z} := G(\mathbf{z}), \\ \text{s.t.} \quad & \mathbf{z} \geq \mathbf{0} \end{aligned} \quad (26)$$

where

$$\mathbf{z} = \begin{bmatrix} \mathbf{u} \\ \mathbf{v} \end{bmatrix}, \quad \mathbf{B} = \begin{bmatrix} \Phi^T \Phi & -\Phi^T \Phi \\ -\Phi^T \Phi & \Phi^T \Phi \end{bmatrix}, \quad \mathbf{c} = \begin{bmatrix} -\Phi^T \mathbf{y} \\ \Phi^T \mathbf{y} \end{bmatrix} + \rho \mathbf{1}^T - \rho \mathbf{w}_z^{t-1}$$

where $\mathbf{1}^T$ represents an all-ones column vector having the same dimension with \mathbf{z} , and $\mathbf{w}_z^{t-1} = [(\mathbf{w}_u^{t-1})^T, (\mathbf{w}_v^{t-1})^T]^T$. Note that \mathbf{w}_z^{t-1} is a subgradient of $\|\mathbf{z}^{t-1}\|_{K,1}$, i.e., $\mathbf{w}_z^{t-1} \in \partial \|\mathbf{z}^{t-1}\|_{K,1}$. Since $\mathbf{z}^{t-1} \geq \mathbf{0}$, a feasible subgradient \mathbf{w}_z^{t-1} can be an indicator vector having either one-valued or zero-valued elements, where the indices for the one-valued elements of \mathbf{w}_z^{t-1} correspond to the indices of the K -largest elements of \mathbf{z}^{t-1} . The problem (26) is an equivalent problem for the subproblem (23). We apply the gradient projection descent method to solve (26), and the k th update is

$$\begin{aligned} \mathbf{z}^{(k+\frac{1}{2})} &= Proj(\mathbf{z}^{(k)} - \alpha^k \nabla G(\mathbf{z}^{(k)})), \\ \mathbf{z}^{(k+1)} &= \mathbf{z}^{(k)} + \beta^k (\mathbf{z}^{(k+\frac{1}{2})} - \mathbf{z}^{(k)}) \end{aligned} \quad (27)$$

where $\alpha^k > 0$ is the step size and it can be determined by the BB step size, which can be calculated as $\alpha^t = \frac{\|\mathbf{z}^k - \mathbf{z}^{k-1}\|^2}{(\mathbf{z}^k - \mathbf{z}^{k-1})^T (G(\mathbf{z}^k) - G(\mathbf{z}^{k-1}))}$; $\beta^k \in (0, 1]$ is another step size to ensure the monotonic-decreasing of objective and it can be calculated in closed-form as $\beta^k = \frac{(\delta^k)^T \nabla G(\mathbf{z}^k)}{(\delta^k)^T \mathbf{B} \delta^k}$, where $\delta^k = \mathbf{z}^{(k+\frac{1}{2})} - \mathbf{z}^{(k)}$ [25]; $Proj(\cdot)$ represents the operation of orthogonal projection that

projects the vector to the nonnegative orthant⁴; $\nabla G(\mathbf{z}^{(k)})$ represents the gradient of $G(\mathbf{z})$ in terms of $\mathbf{z}^{(k)}$. We have $\nabla G(\mathbf{z}^{(k)}) = \mathbf{B}\mathbf{z} + \mathbf{c}$ which can be calculated as

$$\nabla G(\mathbf{z}^{(k)}) = \begin{bmatrix} \Phi^T \Phi (\mathbf{u}^{(k)} - \mathbf{v}^{(k)}) \\ -\Phi^T \Phi (\mathbf{u}^{(k)} - \mathbf{v}^{(k)}) \end{bmatrix} + \begin{bmatrix} -\Phi^T \mathbf{y} \\ \Phi^T \mathbf{y} \end{bmatrix} - \rho \mathbf{w}_z^{t-1} + \rho \mathbf{1}^T. \quad (28)$$

In a nutshell, the proposed algorithm computes the following two steps iteratively until convergence:

$$\begin{aligned} \text{(a)} \quad & \mathbf{w}_z^{t-1} \in \partial \|\mathbf{z}^{t-1}\|_{K,1} \\ \text{(b)} \quad & \mathbf{z}^t = \underset{\mathbf{z} \geq 0}{\operatorname{argmin}} \left\{ \frac{1}{2} \mathbf{z}^T \mathbf{B} \mathbf{z} + \mathbf{c}^T \mathbf{z} \right\} \end{aligned} \quad (29)$$

where \mathbf{z} , \mathbf{B} and \mathbf{c} are defined in (26). The subproblem (b) in (29) is solved by applying the gradient projection descent updates in (27). We summarize this double-loop DC-GPSR algorithm in Algorithm 1.

Algorithm 1 Double-loop DC-GPSR (DIDC-GPSR)

Input: measurements \mathbf{y} , measurement matrix Φ and a small number ϵ

Output: reconstructed $\hat{\mathbf{x}}$

Initialization: $\mathbf{u}^0, \mathbf{v}^0, \mathbf{z}^0 \leftarrow [(\mathbf{u}^0)^T, (\mathbf{v}^0)^T]^T$

- 1: **for** $t = 1, 2, \dots$ **do**
 - 2: Compute a subgradient $\mathbf{w}_z^{t-1} \in \partial \|\mathbf{z}^{t-1}\|_{K,1}$
 - 3: **for** $k = 1, 2, \dots$ **do**
 - 4: Compute gradient $\nabla G(\mathbf{z}^{(k)})$ by (28)
 - 5: Perform gradient projection descent (27) for obtaining $\mathbf{z}^{(k+1)}$
 - 6: Check convergence, set $\mathbf{z}^* \leftarrow \mathbf{z}^{(k+1)}$ and proceed to step 7 if convergence is satisfied; otherwise return to step 3.
 - 7: **end for**
 - 8: $\mathbf{z}^t \leftarrow \mathbf{z}^*$
 - 9: Check terminate condition $\|\mathbf{z}^t - \mathbf{z}^{t-1}\|_2 \leq \epsilon$ and return to Step 1 if not satisfied; otherwise terminate with the solution $\mathbf{z}^t = [(\mathbf{u}^t)^T, (\mathbf{v}^t)^T]^T$, and obtain the reconstruction $\hat{\mathbf{x}} = \mathbf{u}^t - \mathbf{v}^t$
 - 10: **end for**
-

⁴Let $\mathbb{R}_+^n = \{\mathbf{x} = (x_1, x_2, \dots, x_n) | x_1 \geq 0, x_2 \geq 0, \dots, x_n \geq 0\}$ be the nonnegative orthant of \mathbb{R}^n .

V. SINGLE-LOOP DC GRADIENT PROJECTION DESCENT FOR SPARSE RECONSTRUCTION

In the proposed DIDC-GPSR algorithm, at each iteration we solve a nonsmooth convex subproblem (23) using another iterative algorithm, i.e., the gradient projection descent updates. This double-loop computations have high computation complexity. In this section, we derive a closed-form solution to solve the convex subproblem by performing a special DC decomposition to eliminate the inner iterations. Thus, we propose a basic single-loop DC-GPSR algorithm. Interestingly, we show that the proposed basic single-loop DC-GPSR algorithm can be interpreted by simple gradient projection descent updates. Furthermore, we accelerate the single-loop DC-GPSR algorithm using BB step size and propose an extension algorithm for single-loop DC-GPSR.

A. A Basic Single-Loop DC-GPSR Algorithm

We first rewrite the least squares objective of problem (17) in an equivalent form as

$$\frac{1}{2}\|\mathbf{y} - \Phi\mathbf{x}\|_2^2 = \frac{l}{2}\|\mathbf{x}\|_2^2 - \left(\frac{l}{2}\|\mathbf{x}\|_2^2 - \frac{1}{2}\|\mathbf{y} - \Phi\mathbf{x}\|_2^2 \right) \quad (30)$$

where $l \geq 0$ is a Lipschitz constant of the least square objective. By substituting (30) into problem (17), the unconstrained sparse reconstruction problem (17) becomes

$$\min_{\mathbf{x}} \frac{l}{2}\|\mathbf{x}\|_2^2 - \left(\frac{l}{2}\|\mathbf{x}\|_2^2 - \frac{1}{2}\|\mathbf{y} - \Phi\mathbf{x}\|_2^2 \right) + \rho(\|\mathbf{x}\|_1 - \|\mathbf{x}\|_{K,1}) := F(\mathbf{x}). \quad (31)$$

Then, we perform the following DC decomposition on the objective in problem (31), and have

$$\min_{\mathbf{x}} \underbrace{\frac{l}{2}\|\mathbf{x}\|_2^2 + \rho\|\mathbf{x}\|_1}_{f(\mathbf{x})} - \underbrace{\left(\frac{l}{2}\|\mathbf{x}\|_2^2 - \frac{1}{2}\|\mathbf{y} - \Phi\mathbf{x}\|_2^2 + \rho\|\mathbf{x}\|_{K,1} \right)}_{g(\mathbf{x})} := F(\mathbf{x}), \quad (32)$$

where $f(\mathbf{x})$ and $g(\mathbf{x})$ are two convex functions. The convexity of $g(\mathbf{x})$ can be ensured by confirming the convexity of $\frac{l}{2}\|\mathbf{x}\|_2^2 - \frac{1}{2}\|\mathbf{y} - \Phi\mathbf{x}\|_2^2$, which is given in Theorem 2.

Theorem 2: The least squares objective $\frac{1}{2}\|\mathbf{y} - \Phi\mathbf{x}\|_2^2$ is smooth and its gradient function is Lipschitz continuous with the Lipschitz constant $l = \lambda_{\max}(\Phi^T\Phi)$, where $\lambda_{\max}(\cdot)$ denotes the maximum eigenvalue of a matrix. Thus, the function $h(\mathbf{x}) = \frac{l}{2}\|\mathbf{x}\|_2^2 - \frac{1}{2}\|\mathbf{y} - \Phi\mathbf{x}\|_2^2$ for $l = \lambda_{\max}(\Phi^T\Phi)$ is convex.

Prove: See Appendix B.

By writing the ℓ_2 -square terms in (32) into standard quadratic forms, we have

$$\min_{\mathbf{x}} \underbrace{\frac{l}{2}\mathbf{x}^T\mathbf{x} + \rho\|\mathbf{x}\|_1}_{f(\mathbf{x})} - \underbrace{\left(\frac{l}{2}\mathbf{x}^T\mathbf{x} - \frac{1}{2}\mathbf{x}^T\Phi^T\Phi\mathbf{x} + (\Phi^T\mathbf{y})^T\mathbf{x} + \rho\|\mathbf{x}\|_{K,1} \right)}_{g(\mathbf{x})} := F(\mathbf{x}). \quad (33)$$

We split the positive and negative part of \mathbf{x} by letting $\mathbf{u} = (\mathbf{x})_+$, $\mathbf{v} = (-\mathbf{x})_+$. Denoting $\mathbf{z} = [\mathbf{u}^T, \mathbf{v}^T]^T$, we express (33) as

$$\begin{aligned} \min_{\mathbf{z}} \quad & \underbrace{\frac{l}{2}\mathbf{z}^T\mathbf{z} + \rho\mathbf{1}^T\mathbf{z}}_{f(\mathbf{z})} - \underbrace{\left(\frac{l}{2}\mathbf{z}^T\mathbf{z} - \frac{1}{2}\mathbf{z}^T\mathbf{B}\mathbf{z} + \mathbf{q}^T\mathbf{z} + \rho\mathbf{1}_K^T\mathbf{z}\right)}_{g(\mathbf{z})} := F(\mathbf{z}) \\ \text{s.t.} \quad & \mathbf{z} \geq 0 \end{aligned} \quad (34)$$

where

$$\mathbf{z} = \begin{bmatrix} \mathbf{u} \\ \mathbf{v} \end{bmatrix}, \quad \mathbf{B} = \begin{bmatrix} \Phi^T\Phi & -\Phi^T\Phi \\ -\Phi^T\Phi & \Phi^T\Phi \end{bmatrix}, \quad \mathbf{q} = \begin{bmatrix} \Phi^T\mathbf{y} \\ -\Phi^T\mathbf{y} \end{bmatrix},$$

and $\mathbf{1}_K$ is the indicator vector having either one-valued or zero-valued elements, and the one-valued elements of $\mathbf{1}_K$ indicate the K largest elements of \mathbf{z} . Following the DC algorithm framework to solve problem (34), we perform the following two steps repeatedly until convergence:

$$\begin{aligned} \text{(a)} \quad & \partial g(\mathbf{z}^{t-1}) = l\mathbf{z}^{t-1} - \mathbf{B}\mathbf{z}^{t-1} + \mathbf{q} + \rho\mathbf{1}_K^{t-1} \\ \text{(b)} \quad & \mathbf{z}^t = \underset{\mathbf{z} \geq 0}{\operatorname{argmin}} \left\{ \frac{l}{2}\mathbf{z}^T\mathbf{z} + \rho\mathbf{1}^T\mathbf{z} - \mathbf{z}^T\partial g(\mathbf{z}^{t-1}) \right\} \end{aligned} \quad (35)$$

where the superscript $t-1$ and t respectively indicate the $(t-1)$ th and the t th update. The subproblem (b) of (35) has a closed-form optimal solution. To derive it, we rewrite the subproblem (b) of (35) as

$$\begin{aligned} \min_{\mathbf{z}} \quad & \frac{l}{2}\mathbf{z}^T\mathbf{z} + \rho\mathbf{z}^T\mathbf{1} - \mathbf{z}^T\partial g(\mathbf{z}^{t-1}) \\ \text{s.t.} \quad & \mathbf{z} \geq 0. \end{aligned} \quad (36)$$

where

$$\partial g(\mathbf{z}^{t-1}) = l\mathbf{z}^{t-1} - \mathbf{B}\mathbf{z}^{t-1} + \mathbf{q} + \rho\mathbf{1}_K^{t-1}.$$

The problem (36) can be expressed as

$$\begin{aligned} \min_{\mathbf{z}} \quad & \frac{l}{2}\|\mathbf{z} - \frac{1}{l}(\partial g(\mathbf{z}^{t-1}) - \rho\mathbf{1})\|_2^2 \\ \text{s.t.} \quad & \mathbf{z} \geq 0. \end{aligned} \quad (37)$$

The problem (37) is to minimize the $\|\mathbf{z} - \frac{1}{l}(\partial g(\mathbf{z}^{t-1}) - \rho\mathbf{1})\|_2^2$ over $\mathbf{z} \geq 0$ with respect to variable \mathbf{z} . The solution is simply the Euclidean projection of $\frac{1}{l}(\partial g(\mathbf{z}^{t-1}) - \rho\mathbf{1})$ onto the nonnegative orthant. Thus, the gradient projection descent update has a closed-form optimal solution

$$\begin{aligned} \mathbf{z}^* &= \operatorname{Proj} \left(\frac{1}{l}(\partial g(\mathbf{z}^{t-1}) - \rho\mathbf{1}) \right) \\ &= \left(\frac{1}{l}(\partial g(\mathbf{z}^{t-1}) - \rho\mathbf{1}) \right)_+ \end{aligned} \quad (38)$$

where the $Proj(\cdot)$ represents the Euclidean projection onto the feasible set $\mathbf{z} \geq 0$, which is simply the positive-taking operation denoted by $(\cdot)_+$. Using the closed-form solution (38) for the subproblem (b) of (35), the DC programming procedure (35) is simplified to perform the following two single-step computations repeatedly until convergence:

$$\begin{aligned} \text{(a)} \quad & \partial g(\mathbf{z}^{t-1}) = l\mathbf{z}^{t-1} - \mathbf{B}\mathbf{z}^{t-1} + \mathbf{q} + \rho\mathbf{1}_K^{t-1} \\ \text{(b)} \quad & \mathbf{z}^t = \left(\frac{1}{l}(\partial g(\mathbf{z}^{t-1}) - \rho\mathbf{1}) \right)_+ . \end{aligned} \quad (39)$$

Thus, we summarize the updates (39) as a single-loop DC gradient projection algorithm in Algorithm 2. By avoiding the inner-loop iterations, the computation complexity of Algorithm 2 for each iteration is largely reduced compared to Algorithm 1. However, we comment that if the parameter l is large, Algorithm 2 can be slow to convergence. Therefore, we will further propose an accelerated algorithm in the following section.

Algorithm 2 Single-loop DC-GPSR-Basic (SIDC-GPSR-Basic)

Input: measurements \mathbf{y} , measurement matrix Φ and a small number ϵ

Output: reconstructed $\hat{\mathbf{x}}$

Initialization: $\mathbf{u}^0, \mathbf{v}^0, \mathbf{z}^0 \leftarrow [(\mathbf{u}^0)^T, (\mathbf{v}^0)^T]^T$

- 1: **for** $t = 1, 2, \dots$ **do**
 - 2: Compute the gradient $\partial g(\mathbf{z}^{t-1}) = l\mathbf{z}^{t-1} - \mathbf{B}\mathbf{z}^{t-1} + \mathbf{q} + \rho\mathbf{1}_K^{t-1}$ as (a) in (39)
 - 3: Perform the optimal projection operation $\mathbf{z}^t = \left(\frac{1}{l}(\partial g(\mathbf{z}^{t-1}) - \rho\mathbf{1}) \right)_+$ as (b) in (39)
 - 4: Check terminate condition $\|\mathbf{z}^t - \mathbf{z}^{t-1}\|_2 \leq \epsilon$, return to step 1 if not satisfied; otherwise terminate with the solution $\mathbf{z}^t = [(\mathbf{u}^t)^T, (\mathbf{v}^t)^T]^T$, and return the reconstruction $\hat{\mathbf{x}} = \mathbf{u}^t - \mathbf{v}^t$
 - 5: **end for**
-

B. An Extension Algorithm for Single-loop DC-GPSR Using Monotonic BB Step Size

A crucial observation of Algorithm 2 (SIDC-GPSR-Basic algorithm) is that we can interpret it as a simple projection gradient descent method to solve a nonconvex optimization problem with global convergence guarantee. This observation can be obtained by substituting the $\partial g(\mathbf{z}^{t-1})$ in

(a) into (b) of (39) such that Step 2 and Step 3 in Algorithm 2 can be combined as the t th update of \mathbf{z}^t

$$\begin{aligned}\mathbf{z}^t &= Proj \left(\mathbf{z}^{t-1} - \frac{1}{l} (\mathbf{B}\mathbf{z}^{t-1} - \mathbf{q} - \rho\mathbf{1}_K^{t-1} + \rho\mathbf{1}) \right) \\ &= \left(\mathbf{z}^{t-1} - \frac{1}{l} (\mathbf{B}\mathbf{z}^{t-1} - \mathbf{q} - \rho\mathbf{1}_K^{t-1} + \rho\mathbf{1}) \right)_+\end{aligned}\quad (40)$$

where the projection operation is simply a nonnegative-clipper operation $(\cdot)_+$. Thus, we can clearly see that the SIDC-GPSR-Basic is a pure gradient projection descent method to solve the following nonconvex problem with the step size $1/l$ for $l = \lambda_{\max}(\Phi^T\Phi)$,

$$\begin{aligned}\min_{\mathbf{z}} \quad & \frac{1}{2}\mathbf{z}^T\mathbf{B}\mathbf{z} - \mathbf{q}^T\mathbf{z} - \rho\mathbf{1}_K^T\mathbf{z} + \rho\mathbf{1}^T\mathbf{z} := F(\mathbf{z}) \\ \text{s.t.} \quad & \mathbf{z} \geq 0\end{aligned}\quad (41)$$

where

$$\mathbf{z} = \begin{bmatrix} \mathbf{u} \\ \mathbf{v} \end{bmatrix}, \quad \mathbf{B} = \begin{bmatrix} \Phi^T\Phi & -\Phi^T\Phi \\ -\Phi^T\Phi & \Phi^T\Phi \end{bmatrix}, \quad \mathbf{q} = \begin{bmatrix} \Phi^T\mathbf{y} \\ -\Phi^T\mathbf{y} \end{bmatrix}.$$

The problem (41) is an equivalent form of the sparse reconstruction problem (17), but it uses a nonnegative double-sized variable $\mathbf{z} = [(\mathbf{x})_+^T, (-\mathbf{x})_+^T]^T$ to express the sparse vector \mathbf{x} . As we have known, the gradient projection is a mature method for convex optimizations. However, it generally cannot directly applies to the nonconvex problem with any convergence guarantee. Interestingly, as a gradient projection descent for nonconvex sparse reconstructions, the proposed SIDC-GPSR-Basic algorithm is guaranteed to converge, because it is derived from the perspective of DC programming and it shares the same global convergence property with the general DC programming algorithms [22].

Although the step size $1/l$ provides global convergence guarantee for SIDC-GPSR-Basic in Algorithm 2, this step size can be too small in practical implementations. We consider to generalize the step size to accelerate the SIDC-GPSR-Basic algorithm. We use α^t to represent a general step size for the $(t+1)$ th update, and extend the update (40) to be a generic gradient projection descent update for problem (41) as

$$\begin{aligned}\tilde{\mathbf{z}}^{t+1} &= Proj \left(\mathbf{z}^t - \alpha^t (\nabla F(\mathbf{z}^t)) \right) \\ &= \left(\mathbf{z}^t - \alpha^t (\mathbf{B}\mathbf{z}^t - \mathbf{q} - \rho\mathbf{1}_K^t + \rho\mathbf{1}) \right)_+\end{aligned}\quad (42)$$

where α^t can be explicitly calculated by the BB step size method as

$$\alpha^t = \frac{\|\mathbf{z}^t - \mathbf{z}^{t-1}\|^2}{(\mathbf{z}^t - \mathbf{z}^{t-1})^T (F(\mathbf{z}^t) - F(\mathbf{z}^{t-1}))}.\quad (43)$$

To prevent the step size being over large, we employ a scaler $\beta^{t+1} \in (0, 1]$ to limit the update so that the objective will descent monotonically

$$\mathbf{z}^{t+1} = \mathbf{z}^t + \beta^t(\tilde{\mathbf{z}}^{t+1} - \mathbf{z}^t). \quad (44)$$

By writing $\tilde{\mathbf{z}}^{t+1} - \mathbf{z}^t$ as $\boldsymbol{\delta}^t$, we can calculate a β^t that can minimize the objective $F(\mathbf{z}^{t+1})$ by

$$\beta^t = \frac{(\boldsymbol{\delta}^t)^T \nabla F(\mathbf{z}^t)}{(\boldsymbol{\delta}^t)^T \mathbf{B} \boldsymbol{\delta}^t}. \quad (45)$$

We summarize the updates (42) and (44) in Algorithm 3 as an extension single-loop DC-GPSR algorithm, which extends the Algorithm 2 using a monotonic BB step size implementation.

Algorithm 3 Single-loop DC-GPSR with monotonic BB step size (SIDC-GPSR-BB)

Input: measurements \mathbf{y} , measurement matrix Φ and a small number ϵ

Output: reconstructed $\hat{\mathbf{x}}$

Initialization: $\mathbf{u}^0, \mathbf{v}^0, \mathbf{z}^0 \leftarrow [(\mathbf{u}^0)^T, (\mathbf{v}^0)^T]^T, \alpha^0$

- 1: **for** $t = 0, 1, 2, \dots$ **do**
 - 2: Compute update $\tilde{\mathbf{z}}^{t+1}$ using (42)
 - 3: Compute step size β^t using (45)
 - 4: Compute update \mathbf{z}^{t+1} using (44)
 - 5: Compute step size α^{t+1} using (43)
 - 6: Check terminate condition $\|\mathbf{z}^{t+1} - \mathbf{z}^t\|_2 \leq \epsilon$, return to step 1 if not satisfied; otherwise terminate with the solution $\mathbf{z}^{t+1} = [(\mathbf{u}^{t+1})^T, (\mathbf{v}^{t+1})^T]^T$ and return the reconstruction $\hat{\mathbf{x}} = \mathbf{u}^{t+1} - \mathbf{v}^{t+1}$
 - 7: **end for**
-

VI. COMPLEXITY ANALYSIS

Time complexity of an algorithm is related to both the convergence rate and the computation cost of each iteration. Theoretical convergence analysis is too complicated to obtain a rate for our proposed algorithms due to the nonconvexity of optimization objective. Nevertheless, numerical results in the next section will sufficiently demonstrate convergence rates of our proposed algorithms. Before presenting numerical results, we analyse the computation cost for each iteration of our proposed algorithms. At the t th iteration, a common operation of our proposed algorithms is to calculate a subgradient of the top- $(K, 1)$ norm for nonnegative vector

\mathbf{z}^{t-1} , i.e., $\partial\|\mathbf{z}\|_{K,1}^{t-1}$. A feasible subgradient computation of top- $(K, 1)$ norm for a nonnegative vector needs sorting elements and taking the indices of K largest elements. This can be done with the time complexity⁵ $O(2n \log(2n))$, where $2n$ is the length of vector \mathbf{z}^{t-1} . Apart from this subgradient computation, the remaining operations mainly contain matrix-vector multiplications, vector inner products, vector sums and scalar-vector multiplications. Computation cost can be estimated by their floating-point operations (flops). Given the vectors $\mathbf{u} \in \mathbb{R}^n$ and $\mathbf{v} \in \mathbb{R}^n$, a scalar ρ , a dense matrix $\Phi \in \mathbb{R}^{m \times n}$, the vector inner product $\mathbf{u}^T \mathbf{v}$ needs $2n - 1$ flops; the matrix-vector multiplication $\Phi \mathbf{v}$ needs $2mn - m$ flops; the scale-vector $\rho \mathbf{u}$ multiplication needs n flops; the vector sum $\mathbf{u} + \mathbf{v}$ needs n flops. The most computational-intensive term is \mathbf{Bz} , which needs $4mn - m + n$ flops.

In the proposed algorithms, DIDC-GPSR is a double-loop algorithm, while SIDC-GPSR-Basic and SIDC-GPSR-BB are single-loop algorithms. For fair comparisons, the computation costs per iteration are estimated for each overall iteration, that is, from step 2 to step 5 for DIDC-GPSR, step 2 and step 3 for SIDC-GPSR-Basic and from step 2 to step 5 for SIDC-GPSR-BB. We assume that an arbitrary DIDC-GPSR iteration has I inner loops⁶. Thus, computation cost of DIDC-GPSR is $I \times O(mn)$, while computation cost of SIDC-GPSR-Basic is $O(mn)$, and computation cost of SIDC-GPSR-BB is $O(mn)$, where n is the dimension of the sparse vector \mathbf{x} , and m is the dimension of measurements \mathbf{y} . Assuming the DIDC-GPSR algorithm also adopts BB step sizes, its computation cost per iteration is I times higher than that of the SIDC-GPSR-BB algorithm. In another words, we can treat SIDC-GPSR-BB as a special case of DIDC-GPSR when forcing the number of inner loops for every outer iteration to be one, i.e., $I = 1$. Although both SIDC-GPSR-Basic and SIDC-GPSR-BB have the same order of computation costs per iteration being $O(mn)$, the SIDC-GPSR-BB has a higher computation cost because it needs to compute the step sizes α^t and β^t in each iteration as shown in (43) and (45). On the contrary, an SIDC-GPSR-Basic algorithm does not calculate any step size and it can be treated as a pure gradient projection descent with the fixed step size $1/l$ as we have shown in (40).

⁵This is a general approximation of sorting a list of numbers, and there can exist other more efficient methods.

⁶The number I can vary in different iterations of DIDC-GPSR

VII. NUMERICAL RESULT

In this section, we evaluate the algorithm performances for the proposed DIDC-GPSR (Algorithm 1) and SIDC-GPSR-BB (Algorithm 3)⁷. For a fair comparison with SIDC-GPSR, we also adopt BB step sizes for the inner loops of DIDC-GPSR. We evaluate the performances of sparse beamspace channel reconstructions by our proposed algorithms, and compare with the performance of conventional ℓ_1 -regularized GPSR algorithm [25]. Then, we evaluate the performances of our proposed algorithms in terms of reconstructing nearly sparse and noisy beamspace channel vectors. Moreover, we reconstruct some MNIST digits for visualizing reconstruction qualities to compare our proposed algorithms with several existing popular sparse reconstruction algorithms including the ℓ_1 -regularized GPSR, ISTA, and OMP. All the simulations were implemented on a desktop computer equipped with 3.2 GHz Intel Core i7-8700 CPUs with 8GB of physical memory using Python 3.

A. Sparse Beamspace Channel Reconstruction

In this subsection, we perform sparse beamspace channel reconstructions using our proposed DIDC-GPSR and SIDC-GPSR-BB algorithm, as well as the conventional ℓ_1 -regularized GPSR algorithm for comparison. We randomly generate a channel vector for a single-antenna user according to the channel model (1), where the number of antennas at the BS is set as 256 and the number of multiple paths is set as three. A sparse beamspace channel vector is obtained through applying a DFT transformation on the generated spatial-domain channel vector. The obtained beamspace channel vector is nearly sparse due to power leakage. To obtain a sparse beamspace channel vector, we keep the 16 elements that have the largest magnitude, and set the rest of elements to zero. Since we stack the real and imaginary part of a beamspace channel vector, the manipulating vector is a real-valued sparse vector having the dimension of 512×1 . The number of measurements is set as 128. The measurement matrix has the dimension of 128×512 and it is drawn randomly from a standard Gaussian distribution. We set $K = 32$ in the DIDC-GPSR and SIDC-GPSR-BB algorithm implementations.

The original sparse beamspace channel and the reconstructions are shown in Fig. 1. We can see that the DIDC-GPSR and SIDC-GPSR-BB algorithm can achieve perfect reconstructions with

⁷As we have shown, the SIDC-GPSR-Basic (Algorithm 2) has an interesting theoretical interpretation as a pure gradient projection algorithm, but the required step size $1/l$ is too small to converge in a reasonable period for our simulation. Therefore, we do not use Algorithm 2 in the simulations.

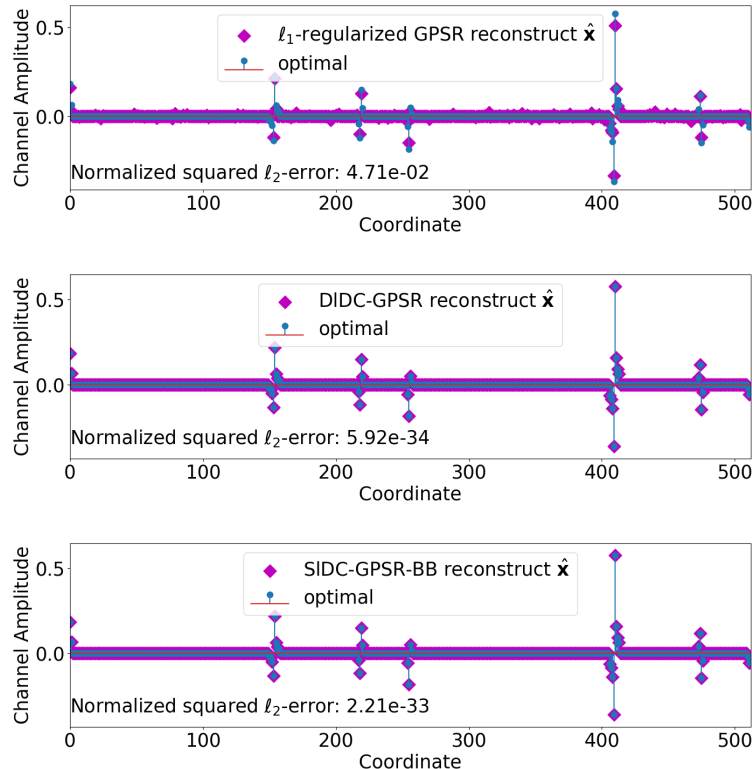


Figure 1: Illustrations of the optimal channel vector and reconstructions

NMSEs 5.92×10^{-34} and 2.21×10^{-33} , whereas the ℓ_1 -regularized GPSR reconstruction has noticeable errors with an NMSE 4.71×10^{-2} . Under the termination condition $\|\hat{\mathbf{x}}^t - \hat{\mathbf{x}}^{t-1}\|_2 \leq 10^{-30}$, the runtimes are about 0.08, 0.08 and 0.05 seconds for ℓ_1 -regularized GPSR, DIDC-GPSR and SIDC-GPSR-BB, respectively. To show their convergence properties during runtimes, we plot objective values versus iterations in Fig. 2, where the objective of proposed DIDC-GPSR and SIDC-GPSR-BB algorithm is $\frac{1}{2}\|\mathbf{y} - \Phi\mathbf{x}\|_2^2 + \rho(\|\mathbf{x}\|_1 - \|\mathbf{x}\|_{K,1})$ while the objective of conventional ℓ_1 -regularized GPSR is $\frac{1}{2}\|\mathbf{y} - \Phi\mathbf{x}\|_2^2 + \rho\|\mathbf{x}\|_1$. For DIDC-GPSR algorithm, the red dots indicate objective values in outer iterations, and the blue solid line shows the objective values along all inner iterations. We can see the proposed DIDC-GPSR algorithm decreases its objective significantly after the seventh outer-step, and approaches the optimal value at the eighth step, whereas the objective of ℓ_1 -regularized GPSR is stuck at a relatively large value. The SIDC-GPSR-BB algorithm has the fastest convergence and can achieve almost the same objective value with DIDC-GPSR algorithm. Then, we investigate the values of least square objective with the ℓ_1 -norm penalty, i.e., $\|\mathbf{y} - \Phi\hat{\mathbf{x}}\|_2^2 + \rho\|\hat{\mathbf{x}}\|_1$, and show the values versus iterations in Fig. 3,

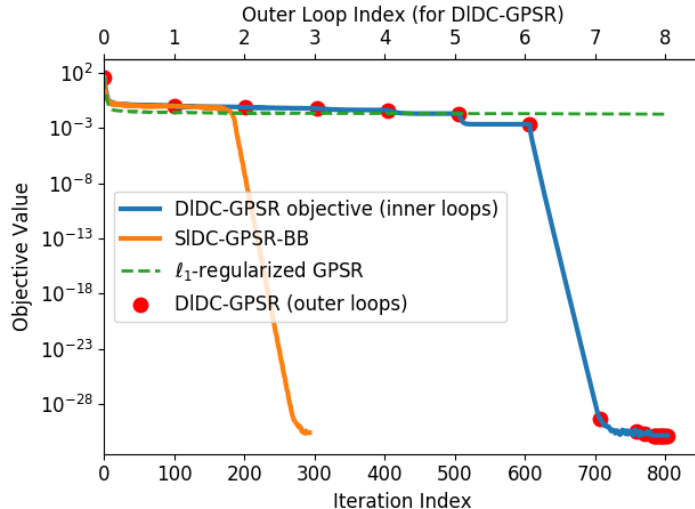


Figure 2: Objective values versus iterations for a beamspace channel reconstruction. Evaluating objective for DIDC-GPSR and SDC-GPSR-BB: $\frac{1}{2}\|\mathbf{y} - \Phi\mathbf{x}\|_2^2 + \rho(\|\mathbf{x}\|_1 - \|\mathbf{x}\|_{K,1})$; Evaluating objective for ℓ_1 -regularized GPSR: $\frac{1}{2}\|\mathbf{y} - \Phi\mathbf{x}\|_2^2 + \rho\|\mathbf{x}\|_1$

where we also plot the optimal values of the penalty term $\rho\|\mathbf{x}_{\text{opt}}\|_1$. We can see that the DIDC-GPSR and SDC-GPSR-BB algorithm arrive and stay at the value of $\rho\|\mathbf{x}_{\text{opt}}\|_1$, which is also the optimal value that the objective $\|\mathbf{y} - \Phi\hat{\mathbf{x}}\|_2^2 + \rho\|\hat{\mathbf{x}}\|_1$ can achieve when $\|\mathbf{y} - \Phi\hat{\mathbf{x}}\|_2^2 = 0$ and $\rho\|\hat{\mathbf{x}}\|_1 = \rho\|\mathbf{x}_{\text{opt}}\|_1$. However, the ℓ_1 -regularized GPSR cannot achieve this optimal value with a noticeable gap. It is meaningful to observe this gap of minimal objective values between our proposed algorithms and conventional ℓ_1 -regularized GPSR algorithm, because this gap can give us an important insight of the approximation error introduced by relaxing the ℓ_0 -norm to ℓ_1 -norm. Figure 4 shows the normalized squared- ℓ_2 errors ($\|\mathbf{x} - \hat{\mathbf{x}}\|_2^2 / \|\mathbf{x}\|_2^2$) versus iterations for reconstructions. We can see that the DIDC-GPSR and SDC-GPSR-BB algorithm can achieve accurate reconstructions with errors on the order of 10^{-34} and 10^{-33} , which is far more accurate than the reconstruction by conventional ℓ_1 -regularized GPSR algorithm having an error on the order of 10^{-2} .

B. Nearly Sparse and Noisy Beamspace Channel Reconstruction

The beamspace channels can be nearly sparse due to power leakage and also can be noisy. In this subsection, we will evaluate the performances of our proposed algorithms on reconstructing nearly sparse channels and noisy channels. We choose a noisy channel sample $\mathbf{x}_{\text{noisy}} \in \mathbb{R}^{512}$

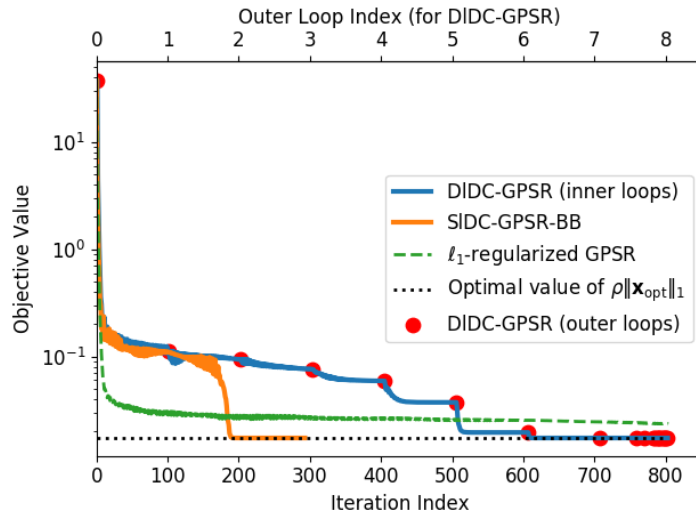


Figure 3: Objective values ($\frac{1}{2}\|\mathbf{y} - \Phi\mathbf{x}\|_2^2 + \rho\|\mathbf{x}\|_1$) versus iterations for a beamspace channel reconstruction

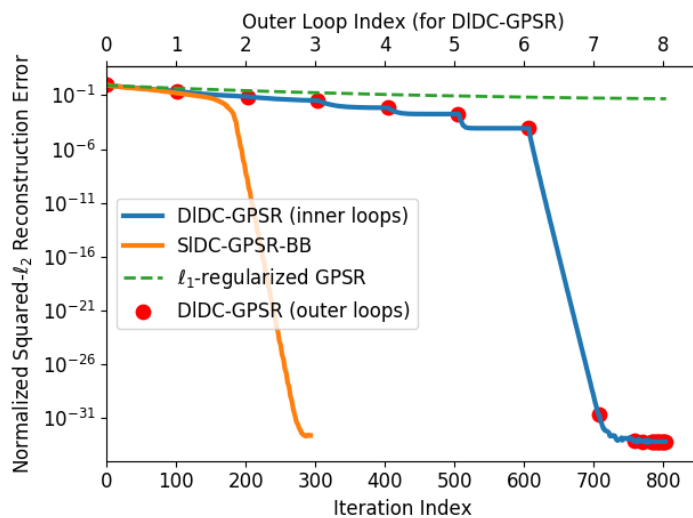
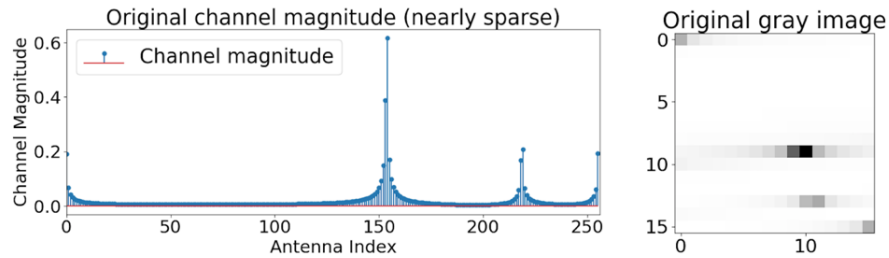
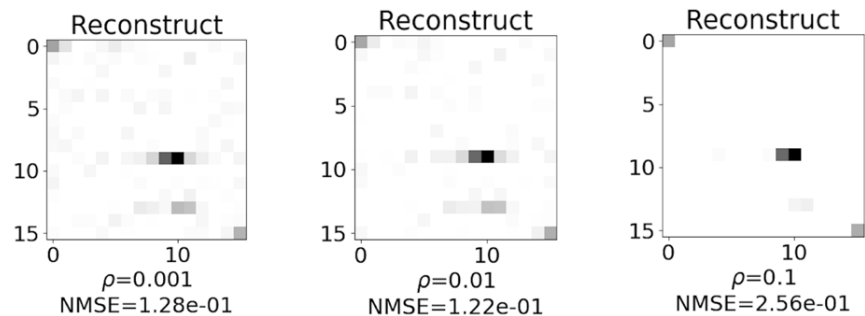


Figure 4: Reconstruction error ($\|\hat{\mathbf{x}} - \mathbf{x}\|_2^2/\|\mathbf{x}\|$) versus iterations in beamspace channel reconstruction

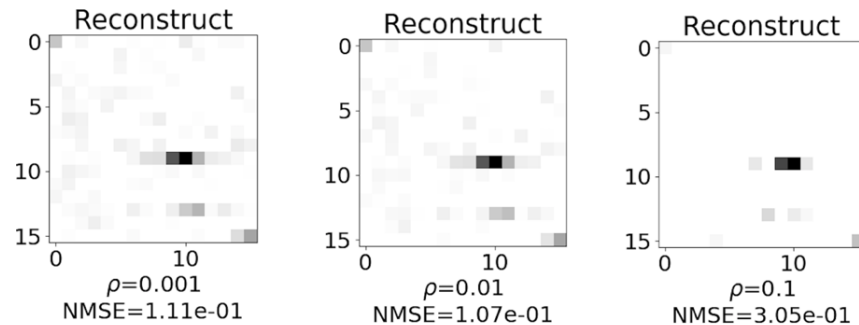
and a nearly sparse channel sample $\mathbf{x}_{\text{approx}} \in \mathbb{R}^{512}$. Then, we perform reconstructions using our proposed algorithms to obtain reconstruction $\hat{\mathbf{x}}$ from the measurements $\mathbf{y}_{\text{noisy}} = \Phi\mathbf{x}_{\text{noisy}}$ and $\mathbf{y}_{\text{approx}} = \Phi\mathbf{x}_{\text{approx}}$, and evaluate the reconstruction performances for different penalty parameters $\rho \in \{0.001, 0.01, 0.1\}$. We plot the original channel magnitudes and illustrate the



(a) Original nearly sparse channel magnitude (left) and 16×16 gray image (right)



(b) DIDC-GPSR reconstructions with different penalty parameter ρ



(c) SIDC-GPSR-BB reconstructions with different penalty parameter ρ

Figure 5: Nearly sparse beamspace channel reconstructions by DIDC-GPSR and SIDC-GPSR-BB for different penalty parameter values

gray images for the magnitudes of original channel and reconstructions. In Fig. 5 (a), we first plot the magnitude of a nearly sparse channel, then we reshape the 256×1 magnitude vector into a 16×16 matrix and draw its gray image. As shown in Fig. 5 (a), a nearly sparse channel has a few large magnitudes but most of the magnitudes are in small values. Figure 5 (b) and Fig. 5 (c) are the reconstruction results with setting the sparsity level $K = 10$ for the DIDC-GPSR and SIDC-GPSR-BB algorithm. We can see that as the penalty parameter ρ becomes larger, the reconstructions becomes sparser. The important elements having large-valued magnitudes can be successfully reconstructed by both the DIDC-GPSR and SIDC-GPSR-BB algorithm. Then,

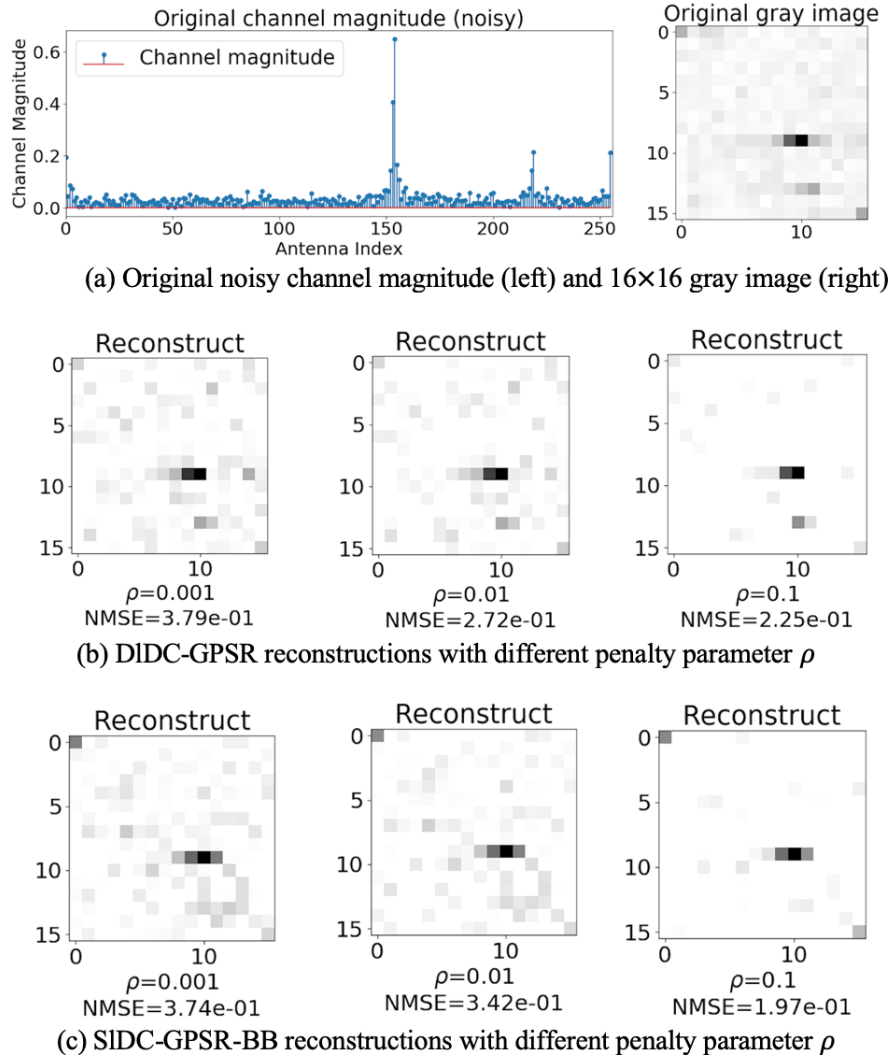


Figure 6: Noisy sparse beamspace channel reconstructions by DIDC-GPSR and SIDC-GPSR-BB for different penalty parameter values

we investigate the reconstruction performances of proposed algorithms on noisy channels. We randomly add AWGN noise on the approximately sparse channels, then we perform reconstructions from the corresponding measurements. A noisy channel for SNR being 5 dB is shown in Fig. 6 (a). The SNR is defined as $\|\mathbf{x}_{noisy}\|_2^2 / \|\mathbf{n}_0\|_2^2$, where $\mathbf{n}_0 \in \mathbb{R}^{256}$ is the added noise vector. Reconstruction results are shown in Fig. 6 (b) and Fig. 6 (c), where the sparsity level is set as $K = 3$ for DIDC-GPSR and SIDC-GPSR-BB. We can see that although reconstruction accuracies degrades due to noise, those important elements having large magnitudes can always be successfully recovered.

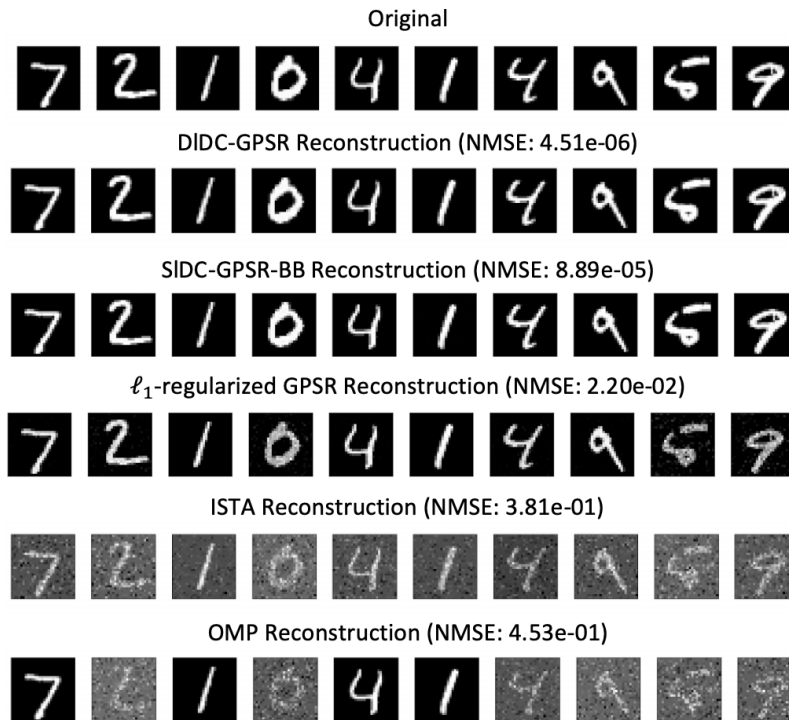


Figure 7: MNIST digits reconstructions by DIDC-GPSR, SIDC-GPSR-BB, ℓ_1 -regularized GPSR, ISTA and OMP algorithms

C. Reconstruction Performance on MNIST Dataset

We have seen the numerical results of sparse reconstructions for beamspace channel vectors, which are generated from a given channel model based on the i.i.d. probabilistic assumption. In this subsection, we will investigate the performances of proposed algorithms on real-world data. We randomly choose 10 handwritten digit images from MNIST dataset to perform reconstructions. Since most of the pixels in an MNIST digit image are zeros, we can treat each image as a sparse signal. Each image has a dimension 28×28 , and we unfold it being a 728 sparse vector. When we perform reconstructions by our proposed DIDC-GPSR and SIDC-GPSR-BB algorithm, we set the top- $(K, 1)$ norm parameter $K = 180$. The dimension of compressed measurements is set as 330. We choose several commonly-used algorithms for comparisons including the ℓ_1 -regularized GPSR, ISTA and OMP algorithms. The original images and reconstructions are shown in Figure 7. We can see that the proposed DIDC-GPSR and SIDC-GPSR-BB algorithm can achieve higher-quality image reconstructions, which have the NMSE 4.15^{-6} and 8.89×10^{-5} , respectively. The benchmark algorithms have higher reconstruction NMSEs. We can visually

see that ℓ_1 -regularized GPSR reconstructs the digits 0, 5, 9 inaccurately; the reconstructions by ISTA are highly noisy; the OMP algorithm reconstructs a few digits clearly, but some digits are seriously blurring. The high reconstruction accuracies by the proposed DIDC-GPSR and SIDC-GPSR-BB verify the robustness of the proposed algorithms on real-world data, which may not follow any i.i.d. probabilistic assumptions. Algorithm runtimes⁸ are shown in Table I. We can see that the SIDC-GPSR-BB and the ℓ_1 -GPSR are faster than the other three algorithms. Considering that the SIDC-GPSR-BB has a higher accuracy than ℓ_1 -GPSR by the order of 10^{-3} , and compared with DIDC-GPSR it has a comparable accuracy but a more than 7 times faster runtime, the SIDC-GPSR-BB has a good tradeoff between reconstruction accuracy and algorithm runtime.

Table I: Runtimes of MNIST digits reconstructions for different algorithms

Algorithm	DIDC-GPSR	SIDC-GPSR-BB	ℓ_1 -GPSR	ISTA	OMP
Runtime (seconds)	9.59	1.29	1.40	12.55	11.89

VIII. CONCLUSION

We proposed three DC programming gradient projection sparse reconstruction algorithms for massive MIMO beamspace channel estimations, and they are DIDC-GPSR (Algorithm 1), SIDC-GPSR-Basic (Algorithm 2) and SIDC-GPSR-BB (Algorithm 3). We derived these algorithms by solving a least squares problem with a nonconvex regularizer. The regularizer is simply the difference between an ℓ_1 -norm and a top- $(K, 1)$ norm, which was introduced to remove the penalties on K largest-magnitude elements. We employed DC programming and gradient projection method to solve the nonconvex sparse reconstruction, and derived different algorithms by different DC decompositions. The proposed double-loop algorithm DIDC-GPSR is straight forward; the single-loop algorithm SIDC-GPSR-Basic has simple updates, and it also shares the theoretical convergence property with the general DC programming method. We observed that the SIDC-GPSR-Basic updates can be perfectly interpreted as a simple gradient projection application. Based on this observation, we proposed an extension algorithm that adopts the BB

⁸The algorithm runtimes were calculated on a desktop computer equipped with 3.2 GHz Intel Core i7-8700 CPU with 8GB of physical memory using Python 3.

step size. The proposed SIDC-GPSR-BB algorithm has a significantly improved convergence rate and can achieve the same level accuracy with the double-loop algorithm DIDC-GPSR. We provide sufficient numerical demonstrations to show the advantages of proposed algorithms such as high accuracies and fast computations. For the future study, we will investigate the theoretical convergence rates of the proposed algorithms.

IX. ACKNOWLEDGEMENT

The authors thank Dr. Hui Ma for his early contribution to Algorithm 1.

APPENDIX

A. Proof of Theorem 1:

Suppose that \mathbf{x}_{ρ^*} is an optimal solution of (17) with given ρ^* , then \mathbf{x}_{ρ^*} is also optimal to (16) as long as $\|\mathbf{x}_{\rho^*}\|_0 \leq K$ (or $\|\mathbf{x}_{\rho^*}\|_1 - \|\mathbf{x}_{\rho^*}\|_{K,1} = 0$) satisfies. Thus, we only need to prove that $\|\mathbf{x}_{\rho^*}\|_0 > K$ is not feasible. Assume \mathbf{x}_{ρ^*} is an optimal solution to (17) with $\rho^* > \max_i \{ |(\Phi^T \mathbf{y})_i| + q(\|\Phi^T \Phi \mathbf{e}_i\|_2 + |(\Phi^T \Phi)_{ii}|/2) \}$. For $\|\mathbf{x}_{\rho^*}\|_0 > K$, we construct a feasible solution to (16) as $\mathbf{x}' = \mathbf{x}_{\rho^*} - x_i \mathbf{e}_i$, where i represents the index of the $(K+1)$ th largest element of vector \mathbf{x}_{ρ^*} ; \mathbf{e}_i represents the unit vector in which the i th element is one while the other elements are zeros; x_i represents the i th element of vector \mathbf{x}_{ρ^*} . By writing the objective of (17) as

$$F(\mathbf{x}) = \frac{1}{2} \mathbf{x}^T \Phi^T \Phi \mathbf{x} - (\Phi^T \mathbf{y})^T \mathbf{x} + \rho^* \|\mathbf{x}\|_1 - \rho^* \|\mathbf{x}\|_{K,1}. \quad (46)$$

We have

$$\begin{aligned} F(\mathbf{x}_{\rho^*}) - F(\mathbf{x}') &= F(\mathbf{x}_{\rho^*}) - F(\mathbf{x}_{\rho^*} - x_i \mathbf{e}_i) \\ &= \frac{1}{2} \mathbf{x}_{\rho^*}^T \Phi^T \Phi \mathbf{x}_{\rho^*} - (\Phi^T \mathbf{y})^T \mathbf{x}_{\rho^*} - \frac{1}{2} (\mathbf{x}_{\rho^*} - x_i \mathbf{e}_i)^T \Phi^T \Phi (\mathbf{x}_{\rho^*} - x_i \mathbf{e}_i) \\ &\quad + (\Phi^T \mathbf{y})^T (\mathbf{x}_{\rho^*} - x_i \mathbf{e}_i) + \rho^* |x_i| \\ &= x_i \mathbf{e}_i^T \Phi^T \Phi \mathbf{x}_{\rho^*} - \frac{1}{2} x_i^2 (\Phi^T \Phi)_{i,i} - x_i (\Phi^T \mathbf{y})_i + \rho^* |x_i| \\ &\geq -x_i \mathbf{e}_i^T \Phi^T \Phi \mathbf{x}_{\rho^*} - \frac{1}{2} x_i^2 (\Phi^T \Phi)_{i,i} - x_i (\Phi^T \mathbf{y})_i + \rho^* |x_i| \\ &\geq -|x_i| \|\mathbf{e}_i^T \Phi^T \Phi\|_2 \|\mathbf{x}_{\rho^*}\|_2 - \frac{1}{2} |x_i| \|\mathbf{x}_{\rho^*}\|_2 |(\Phi^T \Phi)_{i,i}| - |x_i| \cdot |(\Phi^T \mathbf{y})_i| + \rho^* |x_i| \\ &= |x_i| \left(\rho - \|\mathbf{e}_i^T \Phi^T \Phi\|_2 \|\mathbf{x}_{\rho^*}\|_2 - \frac{1}{2} \|\mathbf{x}_{\rho^*}\|_2 |(\Phi^T \Phi)_{i,i}| - |(\Phi^T \mathbf{y})_i| \right) > 0, \quad (47) \end{aligned}$$

which contradicts the assumption that \mathbf{x}_{ρ^*} is an optimal solution to (17).

B. Proof of Theorem 2:

We first derive the Lipschitz constant $l = \lambda_{\max}(\Phi^T \Phi)$, then we prove the convexity of $h(\mathbf{x})$.

We denote the least squares objective by the function $w(\mathbf{x})$. Since the least squares objective $w(\mathbf{x}) = \frac{1}{2} \|\mathbf{y} - \Phi \mathbf{x}\|_2^2$ is smooth if and only if its gradient function is Lipschitz continuous, we assume there exists $l < \infty$, which is named as a Lipschitz constant, such that

$$\|\nabla w(\mathbf{x}) - \nabla w(\mathbf{z})\|_2 \leq l \|\mathbf{x} - \mathbf{z}\|_2. \quad (48)$$

For $w(\mathbf{x}) = \frac{1}{2} \|\mathbf{y} - \Phi \mathbf{x}\|_2^2$, we have

$$\begin{aligned} \|\nabla w(\mathbf{x}) - \nabla w(\mathbf{z})\|_2 &= \|\Phi^T(\Phi \mathbf{x} - \mathbf{y}) - \Phi^T(\Phi \mathbf{z} - \mathbf{y})\|_2 \\ &= \|\Phi^T \Phi (\mathbf{x} - \mathbf{z})\|_2 \\ &\leq \|\|\Phi^T \Phi\|\|_2 \|\mathbf{x} - \mathbf{z}\|_2 \\ &= \lambda_{\max}(\Phi^T \Phi) \|\mathbf{x} - \mathbf{z}\|_2 \end{aligned} \quad (49)$$

where $\|\|\cdot\|\|_2$ represents the spectral norm of a matrix, and $\lambda_{\max}(\cdot)$ represents the largest eigenvalue of a matrix. Thus, we obtain the Lipschitz constant $l = \lambda_{\max}(\Phi^T \Phi)$.

For $h(\mathbf{x}) = \frac{l}{2} \|\mathbf{x}\|_2^2 - \frac{1}{2} \|\mathbf{y} - \Phi \mathbf{x}\|_2^2$, we have the Hessian matrix $\nabla^2 h(\mathbf{x})$ as

$$\begin{aligned} \nabla^2 h(\mathbf{x}) &= \frac{\partial(\nabla h(\mathbf{x}))}{\partial \mathbf{x}} \\ &= \frac{\partial(l\mathbf{x}^T - \Phi^T(\Phi \mathbf{x} - \mathbf{y}))}{\partial \mathbf{x}} \\ &= l\mathbf{I} - \Phi^T \Phi \end{aligned} \quad (50)$$

where \mathbf{I} is the identity matrix. For $l = \lambda_{\max}(\Phi^T \Phi)$, we have $l\mathbf{I} - \Phi^T \Phi \succeq 0$, which means that the Hessian matrix $l\mathbf{I} - \Phi^T \Phi$ of $h(\mathbf{x})$ is semidefinite positive. Thus, $h(\mathbf{x})$ is a convex function of vector \mathbf{x} .

REFERENCES

- [1] W. U. Bajwa, J. Haupt, A. M. Sayeed, and R. Nowak, "Compressed channel sensing: A new approach to estimating sparse multipath channels," *Proc. IEEE*, vol. 98, no. 6, pp. 1058–1076, June 2010.
- [2] S. F. Cotter and B. D. Rao, "Sparse channel estimation via matching pursuit with application to equalization," *IEEE Trans. Commun.*, no. 3, pp. 374–377, Mar. 2002.
- [3] M. R. Raghavendra and K. Giridhar, "Improving channel estimation in OFDM systems for sparse multipath channels," *IEEE Signal Process. Lett.*, no. 1, pp. 52–55, Jan. 2005.
- [4] J. L. Paredes, G. R. Arce, and Z. Wang, "Ultra-wideband compressed sensing: Channel estimation," *IEEE J. Sel. Topics Signal Process.*, no. 3, pp. 383–395, Oct. 2007.

- [5] G. Tauböck, F. Hlawatsch, D. Eiwien, and H. Rauhut, “Compressive estimation of doubly selective channels in multicarrier systems: Leakage effects and sparsity-enhancing processing,” *IEEE J. Sel. Topics Signal Process.*, no. 2, pp. 255–271, Apr. 2020.
- [6] C. R. Berger, S. Zhou, J. C. Preisig, and P. Willett, “Sparse channel estimation for multicarrier underwater acoustic communication: From subspace methods to compressed sensing,” *IEEE Trans. Signal Process.*, no. 3, pp. 1708–1721, Mar. 2020.
- [7] Z. Gao, L. Dai, Z. Wang, and S. Chen, “Spatially common sparsity based adaptive channel estimation and feedback for FDD massive MIMO,” *IEEE Trans. Signal Process.*, vol. 63, no. 23, pp. 6169–6183, Dec. 2015.
- [8] Z. Gao, L. Dai, W. Dai, B. Shim, and Z. Wang, “Structured compressive sensing-based spatio-temporal joint channel estimation for FDD massive MIMO,” *IEEE Trans. Commun.*, vol. 64, no. 2, pp. 601–617, Feb. 2016.
- [9] C. R. Berger, Z. Wang, J. Huang, and S. Zhou, “Application of compressive sensing to sparse channel estimation,” *IEEE Commun. Mag.*, vol. 48, no. 11, pp. 164–174, Nov. 2010.
- [10] M. E. Eltayeb, T. Y. Al-Naffouri, and H. R. Bahrami, “Compressive sensing for feedback reduction in MIMO broadcast channels,” *IEEE Trans. Commun.*, vol. 62, no. 9, pp. 3209–3222, Sep. 2014.
- [11] J. W. Choi, B. Shim, and S. Chang, “Downlink pilot reduction for massive MIMO systems via compressed sensing,” *IEEE Commun. Lett.*, vol. 19, no. 11, pp. 1889–1892, Nov. 2015.
- [12] C.-C. Tseng, J.-Y. Wu, and T.-S. Lee, “Enhanced compressive downlink CSI recovery for FDD massive MIMO systems using weighted block l_1 -minimization,” *IEEE Trans. Commun.*, vol. 64, no. 3, pp. 1055–1067, Mar. 2016.
- [13] H. Almosa, S. Mosleh, E. Perrins, and L. Liu, “Downlink channel estimation with limited feedback for FDD multi-user massive MIMO with spatial channel correlation,” in *Proc. IEEE ICC*, Kansas City, MO, 2018, pp. 1–6.
- [14] W. Shen, L. Dai, Y. Shi, B. Shim, and Z. Wang, “Joint channel training and feedback for FDD massive MIMO systems,” *IEEE Trans. Veh. Technol.*, vol. 65, no. 10, pp. 8762–8767, Oct. 2016.
- [15] X. Rao and V. K. N. Lau, “Distributed compressive CSIT estimation and feedback for FDD multi-user massive MIMO systems,” *IEEE Trans. Signal Process.*, vol. 62, no. 12, pp. 3261–3271, June 2014.
- [16] A. Liu, F. Zhu, and V. K. N. Lau, “Closed-loop autonomous pilot and compressive CSIT feedback resource adaptation in multi-user FDD massive MIMO systems,” *IEEE Trans. Signal Process.*, vol. 65, no. 1, pp. 173–183, Jan. 2017.
- [17] J. Brady, N. Behdad, and A. M. Sayeed, “Beamspace MIMO for millimeter-wave communications: System architecture, modeling, analysis, and measurements,” *IEEE Trans. Antennas Propag.*, vol. 61, no. 7, pp. 3814–3827, July 2013.
- [18] Z. Gao, C. Hu, L. Dai, and Z. Wang, “Channel estimation for millimeter-wave massive MIMO with hybrid precoding over frequency-selective fading channels,” *IEEE Commun. Lett.*, vol. 20, no. 6, pp. 1259–1262, June 2016.
- [19] X. Gao, L. Dai, S. Han, C. I, and X. Wang, “Reliable beamspace channel estimation for millimeter-wave massive MIMO systems with lens antenna array,” *IEEE Trans. Wireless Commun.*, vol. 16, no. 9, pp. 6010–6021, Sep. 2017.
- [20] J. Rodríguez-Fernández, N. González-Prelcic, K. Venugopal, and R. W. Heath, “Frequency-domain compressive channel estimation for frequency-selective hybrid millimeter wave MIMO systems,” *IEEE Trans. Wireless Commun.*, vol. 17, no. 5, pp. 2946–2960, May 2018.
- [21] J. P. González-Coma, J. Rodríguez-Fernández, N. González-Prelcic, L. Castedo, and R. W. Heath, “Channel estimation and hybrid precoding for frequency selective multiuser mmWave MIMO systems,” *IEEE J. Sel. Topics Signal Process.*, vol. 12, no. 2, pp. 353–367, May 2018.
- [22] H. A. L. Thi and T. P. Dinh, “DC programming and DCA: Thirty years of developments,” *Math. Program.*, pp. 5–68, 2018.
- [23] S.-J. Kim, K. Koh, M. Lustig, S. Boyd, and D. Gorinevsky, “An interior-point method for large-scale ℓ_1 -regularized least squares,” *IEEE J. Sel. Topics Signal Process.*, no. 4, pp. 606–617, Dec. 2007.

- [24] W. Yin, S. Osher, D. Goldfarb, and J. Darbon, "Bregman iterative algorithms for ℓ_1 -minimization with applications to compressed sensing," *SIAM Journal on Imaging Sciences*, no. 1, pp. 143–168, 2008 Mar.
- [25] M. A. T. Figueiredo, R. D. Nowak, and S. J. Wright, "Gradient projection for sparse reconstruction: Application to compressed sensing and other inverse problems," *IEEE J. Sel. Topics Signal Process.*, vol. 1, no. 4, pp. 586–597, Dec 2007.
- [26] S. J. Wright, R. D. Nowak, and M. A. T. Figueiredo, "Sparse reconstruction by separable approximation," *IEEE Trans. Signal Process.*, vol. 57, no. 7, pp. 2479–2493, July 2009.
- [27] T. Blumensath and M. E. Davies, "Iterative thresholding for sparse approximations," *Journal of Fourier Analysis and Applications*, vol. 14, pp. 629–654, 2008.
- [28] A. Beck and M. Teboulle, "A fast iterative shrinkage-thresholding algorithm for linear inverse problems," *SIAM J. Imag. Sci.*, vol. 2, no. 1, pp. 183–202, 2009.
- [29] S. Foucart and M.-J. Lai, "Sparsest solutions of underdetermined linear systems via ℓ_q -minimization for $0 \leq q \leq 1$," *Appl. Comput. Harmonic Anal.*, no. 3, pp. 395–407, 2009.
- [30] G. Gasso, A. Rakotomamonjy, and S. Canu, "Recovering sparse signals with a certain family of nonconvex penalties and DC programming," *IEEE Trans. Signal Process.*, no. 12, pp. 4686–4698, Dec. 2009.
- [31] Y. C. Pati, R. Rezaifar, and P. S. Krishnaprasad, "Orthogonal matching pursuit: recursive function approximation with applications to wavelet decomposition," in *Conf. Rec. 27th Asilomar Conf. Signals, Syst. Comput.*, vol. 1, 1993, pp. 40–44.
- [32] J. A. Tropp and A. C. Gilbert, "Signal recovery from random measurements via orthogonal matching pursuit," *IEEE Trans. Inform. Theory*, vol. 53, no. 12, pp. 4655–4666, Dec. 2007.
- [33] D. Needell and J. A. Tropp, "CoSaMP: Iterative signal recovery from incomplete and inaccurate samples," *Applied and Computational Harmonic Analysis*, vol. 26, no. 3, pp. 301–321, 2008.
- [34] B. Efron, T. Hastie, I. Johnstone, and R. Tibshirani, "Least angle regression," *The Annals of Statistics*, vol. 32, no. 2, pp. 407–499, 2004.
- [35] J. Gotoh, A. Takeda, and K. Tono, "DC formulations and algorithms for sparse optimization problems," *Mathematical Programming*, vol. 169, no. 1, pp. 141–176, 2018.
- [36] P. Wu, H. Ma, and J. Cheng, "Sparse channel reconstruction with nonconvex regularizer via DC programming for massive MIMO systems," in *2020 IEEE Globecom*, Taipei, Taiwan, Dec. 2020.
- [37] D. Tse and V. Pramod, *Fundamentals of Wireless Communication*. Cambridge, U.K.: Cambridge Univ. Press, 2005.
- [38] R. W. Heath, N. González-Prelcic, S. Rangan, W. Roh, and A. M. Sayeed, "An overview of signal processing techniques for millimeter wave MIMO systems," *IEEE J. Sel. Topics Signal Process.*, vol. 10, no. 3, pp. 436–453, Apr. 2016.
- [39] I. Rish and G. Y. Grabarnik, *Sparse Modeling: Theory, Algorithms, and Applications*. Boca Raton, Florida: Chapman & Hall/CRC Press, 2015.